Precipitate statistics in an Al-Mg-Si-Cu alloy from scanning precession electron diffraction data

IOP Conf. Series: Journal of Physics: Conf. Series **902** (2017) 012022 doi:10.1088/1742-6596/902/1/012022

Precipitate statistics in an Al-Mg-Si-Cu alloy from scanning precession electron diffraction data

J K Sunde[1], Ø Paulsen[1], S Wenner[1] and R Holmestad[1]

[1]Department of Physics, Norwegian University of Science and Technology (NTNU), Høgskoleringen 5, N-7491 Trondheim, Norway

E-mail: jonas.k.sunde@ntnu.no

Abstract. The key microstructural feature providing strength to age-hardenable Al alloys is nanoscale precipitates. Alloy development requires a reliable statistical assessment of these precipitates, in order to link the microstructure with material properties. Here, it is demonstrated that scanning precession electron diffraction combined with computational analysis enable the semi-automated extraction of precipitate statistics in an Al-Mg-Si-Cu alloy. Among the main findings is the precipitate number density, which agrees well with a conventional method based on manual counting and measurements. By virtue of its data analysis objectivity, our methodology is therefore seen as an advantageous alternative to existing routines, offering reproducibility and efficiency in alloy statistics. Additional results include improved qualitative information on phase distributions. The developed procedure is generic and applicable to any material containing nanoscale precipitates.

1. Introduction

6xxx series Al(-Mg-Si(-Cu)) alloys form an important group of engineering alloys and are found in a range of applications in buildings and constructions, transportation and marine structures. Increasing industrial demand for materials combining properties such as low weight, high strength, high formability and good corrosion resistance, make Al-based alloys prime candidates for future applications. As an example, this is reflected in their growing impact in the automotive industry [1].

The 6xxx series alloys are characterised by a significant increase in hardness upon short-term thermal ageing. This increase is caused by a large number of small, semi-coherent and metastable needle-shaped precipitates formed along the $\langle 100 \rangle_{\mathrm{Al}}$ directions in the Al matrix from a solid solution of Mg and Si [2]. These nanostructures act as obstacles to dislocation movement through the Al matrix, hence strengthening the material.

The early-stage precipitation sequence in Al-Mg-Si-Cu alloys is normally given as [3–5]

$$\mathrm{SSSS} \rightarrow \text{atomic clusters} \rightarrow \text{GP-zones} \rightarrow \beta'', \mathrm{L} \rightarrow \beta'(\text{-Cu}), \mathrm{U1}, \mathrm{U2}, \mathrm{C}, \mathrm{B}', \mathrm{Q}'.$$

The number and type of the different phases forming throughout the Al matrix are crucially dependent on alloy composition and all prior thermo-mechanical processing. In order to further optimise material properties, detailed and reliable precipitate statistics and its change versus different ageing times, is needed. This is generally acquired through bright-field (BF) and/or dark-field (DF) transmission electron microscopy (TEM) imaging techniques, with subsequent

manual counting and measurements [6]. With recent developments of TEM techniques yielding large, multi-dimensional datasets [7], and corresponding parallel advancements in powerful data processing tools [8], techniques for obtaining the statistics in more objective and reproducible manners are sought. This forms the main motivation behind this work.

2. Materials and methods

The material studied has a nominal composition Al-1.11Mg-0.50Si-0.16Cu (at.%) [9]. From an extruded rod with cylindrical profile (Ø 20 mm) a sample of 10 mm height was cut and solution heat treated at 540 °C for 15 min, before water quenched to room temperature. After 4 h natural ageing it was artificially aged for 6 h at 200 °C, yielding a slightly over-aged condition. TEM samples were made by standard electro-polishing using a Struers Tenupol-5.

Scanning precession electron diffraction (SPED) was performed using a NanoMEGAS DigiSTAR scan generator fitted to a JEOL 2100F TEM operated at 200 kV, with a precession angle of 1° and a step size of 2.28 nm. To get high quality data from the nm-sized precipitates the precession system was aligned using the procedure proposed by Barnard et al. [10]. The main SPED dataset is presented as a virtual dark-field (VDF) image (Figure 1) formed by plotting the intensity of a sub-set of pixels in each PED pattern as a function of probe position. The dataset comprises 247 500 diffraction patterns (DPs) covering an area of $1.34\,\mu m^2$ in 550×450 pixels. The 4D-SPED dataset was primarily analysed using the HyperSpy [8] Python library. An image that highlights the precipitate cross-sections was obtained through principal component analysis, giving a component pattern that closely resembled the sum of precipitate-characteristic reflections. After applying local intensity thresholding, the number of precipitate cross-sections in the scanned area was obtained using a blob-detection algorithm based on the Laplacian of Gaussian method on the pre-processed image. Information on precipitate types was extracted using non-negative matrix factorisation (NMF) with a navigation mask surrounding all precipitate cross-sections detected (Figure 2). The NMF component patterns were compared to (kinematically) simulated DPs of reported phases in the Al-Mg-Si-Cu system. High-angle annular dark-field scanning TEM (HAADF-STEM) images were acquired on a double corrected JEOL ARM200CF microscope operated at 200 kV.

The total area analysed by conventional methods covered approximately $1.1\,\mu m^2$, comparable to the SPED scan area, and was acquired in the same grain. The precipitate number density, ρ [μm^{-3}], was calculated as [6]

$$\rho = \frac{3N_{\parallel}}{A(t + \langle l \rangle)}. \tag{1}$$

Here, $N_{\parallel}$ is the number of precipitate cross-sections in the imaged area, A, while t is the area thickness and $\langle l \rangle$ is the average needle length. The factor 3 accounts for the 3 equivalent $\langle 100 \rangle_{Al}$ directions in which the needles grow, hence assuming an isotropic distribution. The sample thickness, measured by electron energy loss spectroscopy (EELS), gives the highest contribution to the uncertainty in the calculated precipitate number density. The total precipitate number density, $\langle \rho \rangle$, is given as the average of all number densities calculated from single images.

3. Results and discussion

The statistics obtained using conventional and SPED methodologies are presented in Table 1, showing a number density of $(65\,700 \pm 6700)\,\mu m^{-3}$ and $(67\,800 \pm 5500)\,\mu m^{-3}$ for the two approaches, respectively. Considering the high number densities involved, this shows a close agreement between the two methods. It implies that the PED pattern stack has sufficient signal-to-noise ratio to give a number density comparable to that of broad-beam illumination modes.

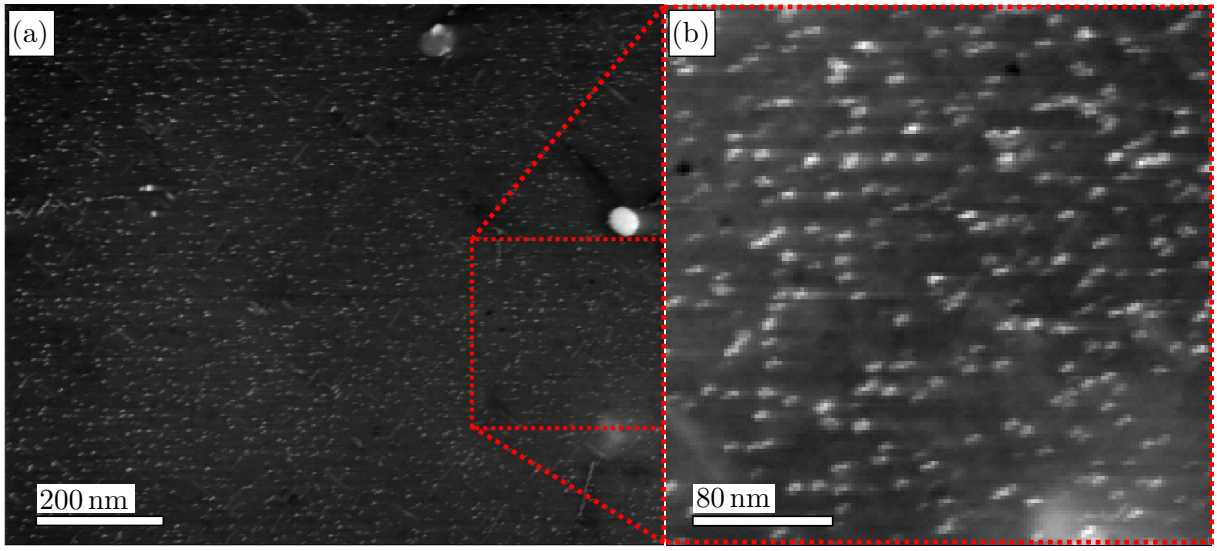

Figure 1. (a) VDF image formed from a SPED scan acquired near a $\langle 100 \rangle_{\mathrm{Al}}$ zone axis using precipitate diffraction spots. The area covers $1.34\,\mu\mathrm{m}^2$ in 550×450 pixels. (b) Enlarged view of the dashed region in (a).

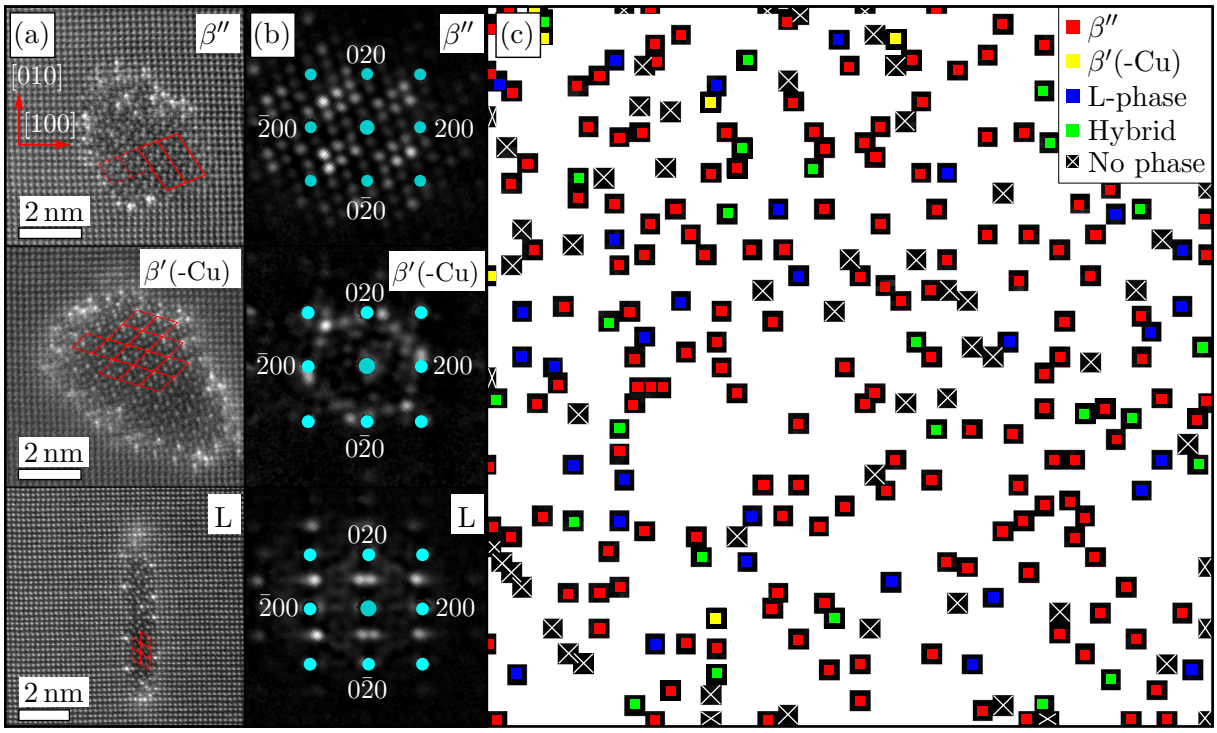

Figure 2. (a) HAADF-STEM images of the three main precipitates observed. Unit cells of the phases are highlighted in red. In the disordered L-phase, parts of the Si-network are marked. (b) NMF component patterns resembling (kinematical) DPs of the corresponding precipitate types in (a). Some aluminium reflections are marked and indexed. (c) Colour-map showing the precipitate phase distribution obtained from loading maps associated with the main NMF component patterns of (b). The area in (c) is the same as in Figure 1 (b).

The transition from Figure 1 (b) to Figure 2 (c) shows how the initial coarse estimate of number density is refined and that in addition, phase fractions are obtained. The latter has excluded those cross-sections which are not associated with a recognisable DP from the phases present. This second refinement is not attainable in manual analysis of BF/DF images where it may be difficult to differentiate between e.g. in-plane and normal orientations of small β'' needles.

Table 1. Precipitate statistics obtained using the two presented methodologies.

Method	β'' [%]	β'(-Cu) [%]	L [%]	Hybrid phase [%]	$\langle\rho\rangle$ [µm^{-3}]
Conventional	54	Unattainable	10	36	65 700±6700
SPED	73	1	12	14	67 800±5500

The precipitate fractions in Table 1 show significant variations, agreeing only on the fractions of the L-phase. This was expected, as the conventional methodology determines precipitate type solely based on shape and orientations relative to the Al matrix, while SPED uses information from reciprocal space. A phase such as β'(-Cu) does normally not extend to the Al interface, and the outer region consists of a narrow layer of other phases (or fractions thereof). Purely geometric considerations must therefore classify less well-defined cross-sections as hybrid. The L-phase has a distinct, narrow cross-section, easily recognised in BF images. Furthermore, since it rarely couples with the other phases, its fraction should be reliable.

4. Conclusions

Computational analysis of SPED data yields precipitate number densities in close agreement to conventional methodologies. Obtained phase fractions show significant deviations between the methods, and is suspected to be a consequence of inaccuracy in traditional routines being based on purely geometric considerations. With implications of equal sensitivity in the two approaches, the SPED estimate of phase fractions is considered more reliable. Due to the increased objectivity of the new analysis, the results are more readily reproducible, which has important implications for the validity and use of TEM statistics in future alloy developments. Further work aims at refining the methodology, making all steps automated and quantifying uncertainties more accurately.

Acknowledgments

All authors extend their gratitude to collaborating researchers Duncan N Johnstone and prof. Paul A Midgley from the University of Cambridge, and prof. Antonius T J van Helvoort from the Norwegian University of Science and Technology.

References

[1] Miller W S, Zhuang L, Bottema J, Wittebrood A J, De Smet P, Haszler A and Vieregge A 2000 *Mater. Sci. Eng.* A **280** 37–49
[2] Totten G E and MacKenzie D S 2003 *Handbook of Aluminium* (New York: Marcel Dekker)
[3] Edwards G A, Stiller K, Dunlop G L and Couper M J 1998 *Acta Mater.* **46** 3893–904
[4] Marioara C D, Andersen S J, Stene T N, Hasting H, Walmsley J, van Helvoort A T J, and Holmestad R 2007 *Phil. Mag.* **87** 3385–413
[5] Ravi C and Wolverton C 2004 *Acta Mater.* **52** 4213–27
[6] Andersen S J 1994 *Metall. Mater. Trans.* A **26** 1931–37
[7] Rauch E F, Portillo J, Nicolopoulos S, Bultreys D, Rouvimov S and Moeck P 2010 *Z. Kristallogr.* **225** 103–9
[8] de la Peña F et al. HyperSpy-1.3 2017 DOI: https://doi.org/10.5281/zenodo.583693
[9] Marioara C D, Andersen S J and Røyset J 2014 *Metall. Mater. Trans.* A **45**, 2938–49
[10] Barnard J S, Johnstone D N and Midgley P A 2017 *Ultramicroscopy* **174** 79–88